Rare Metal Materials and Engineering
Volume 53, Issue 12, December 2024
Available online at www.rmme.ac.cn

Science Press

Cite this article as: Xue Jianchao, Jia Bo, Wang Yafei, et al. Mechanism and Properties of Al_2O_3-Ru Composite Coatings Prepared by Cathode Plasma Electrolytic Deposition[J]. Rare Metal Materials and Engineering, 2024, 53(12): 3306-3312. DOI: 10.12442/j.issn.1002-185X.20240067.

ARTICLE

Mechanism and Properties of Al_2O_3-Ru Composite Coatings Prepared by Cathode Plasma Electrolytic Deposition

Xue Jianchao[1,2], Jia Bo[2], Wang Yafei[2], Feng Qing[2], Chai Zuoqiang[2], Hao Xiaojun[2], Xue Juanqin[1]

[1] College of Metallurgical Engineering, Xi'an University of Architecture and Technology, Xi'an 710055, China; [2] Xi'an Taijin New Energy & Materials Sci-Tech Co., Ltd, Xi'an 710016, China

Abstract: Alumina coatings doped with different precious metals were prepared by cathode plasma electrolytic deposition. Results show that the porosity of precious metal-doped alumina coatings (especially Al_2O_3-Ru) decreases, and the high-temperature cyclic oxidation resistance and spallation resistance are enhanced. The Al_2O_3-Ru composite coating shows better effect: its average oxidation rate K and average amount of oxide spallation G are minimum. Meanwhile, Nernst equation was used to explain the simultaneous deposition of precious metal and alumina, and the whole process and mechanism of deposition were analyzed.

Key words: cathode plasma electrolytic deposition; precious metal; porosity; high-temperature cyclic oxidation resistance; spallation resistance

Al_2O_3 is the most widely applied coating material, which is used in ceramic devices, pharmaceuticals, adsorbents, and carriers. Numerous techniques have been developed to produce Al_2O_3 coatings, including chemical vapor deposition[1], sol-gel[2], evaporation/sputtering[3], and electrophoretic deposition[4]. Plasma electroplating is a combination technique of conventional electrolysis and atmospheric plasma processes[5], which has the advantages of simple operation and high efficiency. Accordingly, plasma electroplating has attracted extensive attention in the fields of protective coating and surface modification.

Plasma electrolysis techniques, such as plasma micro-arc oxidation (PEO) and cathode plasma electroplating deposition (CPED), can be used for the surface treatment of materials[6]. Compared with PEO technique, CPED has wider application prospects. CPED is mainly used for the deposition of metals[7], oxide coatings[8], surface modification/cleaning[9], and pulverizing[10]. Zhou et al[11] deposited different ceramic coatings on different substrates. Wang et al[12] prepared alumina coatings on 304 stainless steel. Bahadori et al[13] investigated the effects of pH value of electrolyte on the Al_2O_3 morphology. Zhang et al[14] used a self-designed cathode plasma arc to deposit the alumina coating on carbon fiber to improve its oxidation resistance.

Wang et al[15] deposited composite Al_2O_3-dispersed Pt thermal barrier coatings on Ni-based superalloy. The coatings significantly improved the high-temperature oxidation resistance and spallation resistance due to the toughening effect of dispersed Pt particles. Isolated and well dispersed micropores could attenuate the stress effect. However, the porosity caused by Pt was costly, thereby reducing the production application.

Aiming to decrease the material cost, precious metals were adopted in this research for coating preparation. Al_2O_3-Ru and Al_2O_3-Pd coatings were deposited on the nickel-based K418 superalloy by CPED from aqueous solutions. The deposition mechanism was studied, and the properties of prepared composite coatings were characterized.

1 Experiment

The schematic diagram of CPED device used for preparing Al_2O_3 coatings is shown in Fig. 1. TN5KGZ01 power unit provided the maximum voltage of 500 V and the maximum current intensity of 30 A in the frequency range of 50–2000

Received date: February 02, 2024
Foundation item: Shaanxi Province Key Research and Development Plan (2024GX-YBXM-368)
Corresponding author: Jia Bo, Senior Engineer, Xi'an Taijin New Energy & Materials Sci-Tech Co., Ltd, Xi'an 710016, P. R. China, E-mail: ppqtmyy@163.com

Hz with the duty ratio range of 0%–90%. The Pt electrode (80 mm×40 mm×0.12 mm) served as the anode and the K418 sample (20 mm×10 mm×3 mm) was used as the cathode. Subsequently, the K418 sample was polished with 400# sandpaper and then ultrasonically cleaned in ethanol for 20 min. The electrolytes consisted of $Al(NO_3)_3·9H_2O$ (analytically pure), polyethylene glycol (PEG, analytically pure), $PdCl_2$ (analytically pure), $RuNO(NO_3)_3$ (analytically pure), $H_2PtCl_6·6H_2O$ (analytically pure), and deionized water. The concentration of $Al(NO_3)_3·9H_2O$, PEG, $PdCl_2$, $RuNO(NO_3)_3$, and $H_2PtCl_6·6H_2O$ was 0.5 mol/L, 25 g/L, 0.0006 mol/L, 0.0006 mol/L, and 0.0006 mol/L, respectively. The process was conducted for 30 min and controlled by a computer. All deposition tests were conducted at the speed of 1 V/s, frequency of 2000 Hz, and duty ratio of 80%. Deposition voltages of 130 and 150 V were used.

The morphologies of Al_2O_3 coatings doped with different precious metal particles were observed by scanning electron microscope (SEM, JMS-6480A) equipped with an energy dispersive X-ray spectroscope (EDS). The porosity of the coatings was evaluated on the basis of the area ratio of pores observed in SEM images.

In order to investigate the kinetics of oxidation resistance and spallation resistance of the coatings, the high-temperature cyclic oxidation experiments were conducted at 1273 K for 100 h. The experiment method was described in Ref.[15].

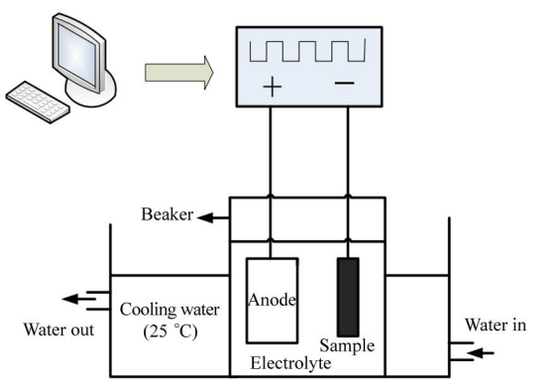

Fig.1 Schematic diagram of CPED device

2 Results and Discussion

2.1 Morphologies

Fig. 2 illustrates the surface morphologies of composite coatings prepared by CPED from aqueous solutions containing 0.5 mol/L $Al(NO_3)_3·9H_2O$ with different precious metal particles. It can be seen that with the increase in voltage, the porosity is decreased and the average diameter of micropores is increased from 10 μm to 25 μm. Besides, after CPED at 150 V, the Al_2O_3-Ru coating is dense, and the pore diameter for Al_2O_3-Ru coating is smaller than that of Al_2O_3-Pd and Al_2O_3-Pt coatings. The porosities of the Al_2O_3-Pt and Al_2O_3-Pd coatings are 12.73% and 9.97%, respectively. The porosity of the Al_2O_3-Ru coating is optimal of 9.01%.

Fig.3 shows SEM surface images at backscattered electron (BSE) mode of composite coatings prepared by CPED with different precious metal particles. EDS analysis result shows that numerous precious metal particles (white spots) are dispersed in the Al_2O_3 coatings. Many precious metal particles are aggregated in the pores after deposition at 130 V. With the increase in voltage, the distribution of precious metal particles becomes more diffused. and the content as well as the particle diameter of the precious metal particles is decreased. Simultaneously, due to the high temperature of plasma, the precious metal ions accept electrons and then crystallize. In this process, micron-scale particles are formed due to

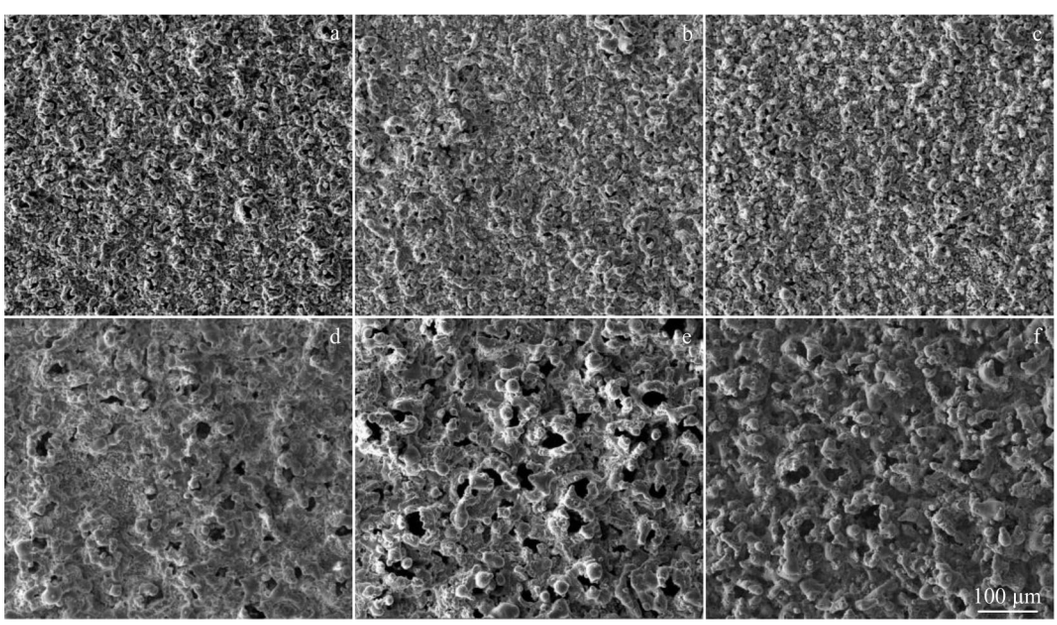

Fig.2 Surface morphologies of different Al_2O_3 coatings prepared by CPED at 130 V (a – c) and 150 V (d – f): (a, d) Al_2O_3-Pd coating, (b, e) Al_2O_3-Ru coating, and (c, f) Al_2O_3-Pt coating

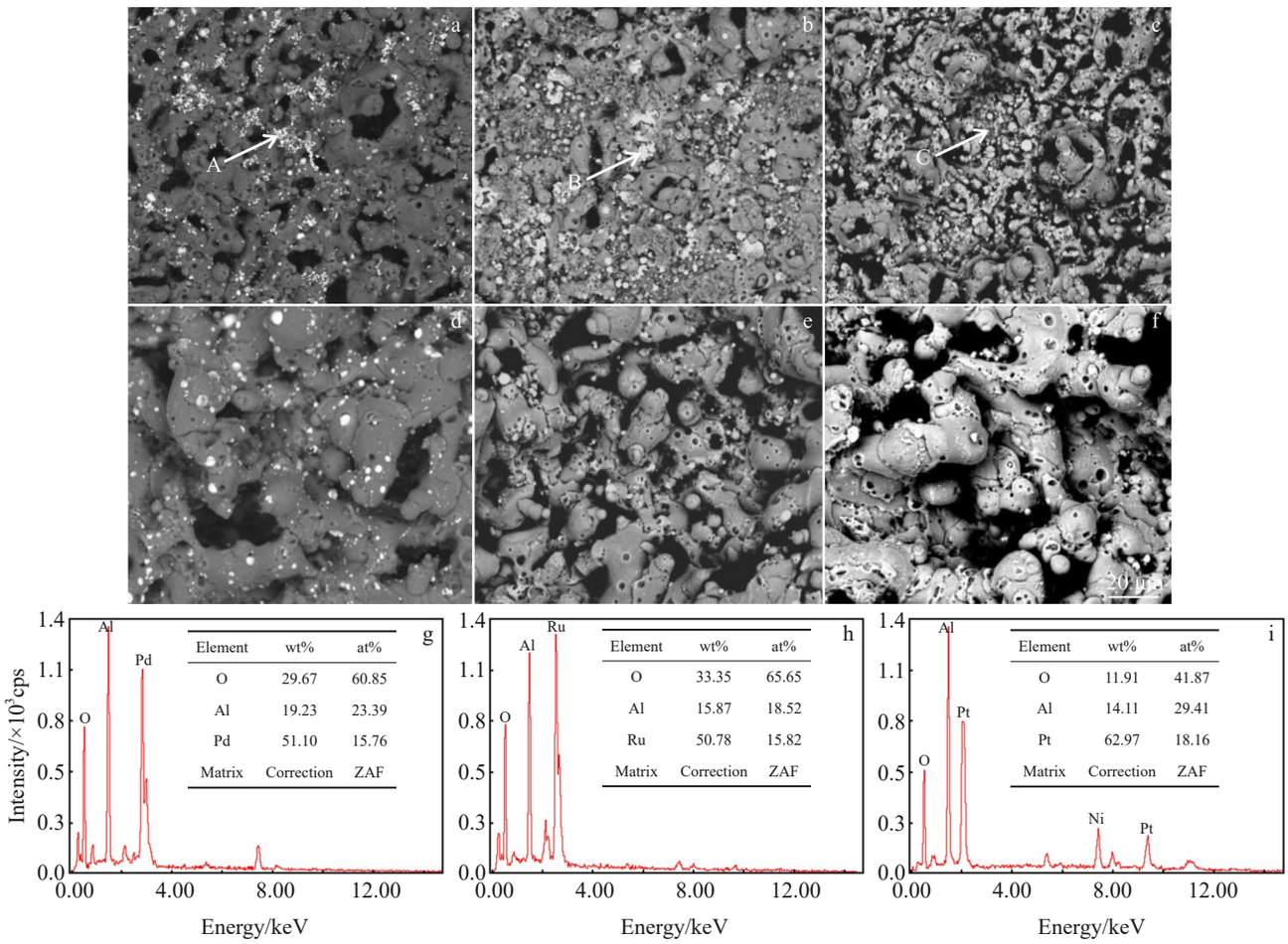

Fig.3 SEM-BSE surface images of different Al_2O_3 coatings prepared by CPED at 130 V (a – c) and 150 V (d – f): (a, d) Al_2O_3-Pd coating, (b, e) Al_2O_3-Ru coating, and (c, f) Al_2O_3-Pt coating; EDS analysis results of point A in Fig. 3a (g), point B in Fig. 3b (h), and point C in Fig.3c (i)

supercooling and surface tension. Nano-sized precious metal particles are dispersed in the Al_2O_3 coatings to absorb free electrons during the breakdown of coatings, preventing the occurrence of electron avalanche breakdown and improving the critical field of composite coatings. Thus, the porosity of the coatings is reduced.

2.2 Deposition mechanism

Table 1 presents the initial concentrations of ions in the electrolytes.

Firstly, the hydrolysis reactions are performed, wherein the ionization reaction proceeds, as follows:

$$Al^{3+}+3H_2O \rightleftharpoons Al(OH)_3+3H^+ \quad (1)$$

$$RuNO(NO_3)_3=(RuNO)^{3+}+3NO_3^- \quad (2)$$

$$PdCl_2=Pd^{2+}+2Cl^- \quad (3)$$

$$H_2PtCl_6\cdot 6H_2O=8H^++Pt^{4+}+6Cl^-+6OH^- \quad (4)$$

The formation reactions of Al_2O_3-Pt, Al_2O_3-Ru, and Al_2O_3-Pd coatings during CPED are complex. The following electrode reactions may occur on the cathode and anode surfaces:

$$2H_2O - 4e^- = O_2 + 4H^+ \quad (5)$$

$$2H^+ + 2e^- = H_2 \quad (6)$$

$$(RuNO)^{3+}+e^-+2O^{2-}=RuO_2+NO \quad (7)$$

$$Pd^{2+}+2e^-=Pd \quad (8)$$

$$Pt^{4+}+4e^-=Pt \quad (9)$$

Table 2 lists the standard electrode potentials for the further calculation process. Nernst equation was used for analysis, as follows:

$$\varphi=\varphi^{\ominus}-\frac{RT}{zF}\ln\frac{(a^{\nu})_{\text{reduction station}}}{(a^{\nu})_{\text{oxidation station}}}+\eta \quad (10)$$

where $\varphi^{\ominus}$ is the standard electrode potential of the electrode reaction; R is the gas constant; T is the Kelvin temperature; z is the charge number; F is the Faraday constant affecting the

Table 1 Initial pH value and concentration of electrolyte ions of different electrolytes

Parameter	$Al(NO_3)_3$-Pd	$Al(NO_3)_3$-Ru	$Al(NO_3)_3$-Pt
pH value	2.13	2.53	2.51
Al^{3+} content/mol·L^{-1}	0.5	0.5	0.5
Pt^{4+} content/mol·L^{-1}	0	0	0.0006
Pd^{2+} content/mol·L^{-1}	0.0006	0	0
$(RuNO)^{3+}$ content/mol·L^{-1}	0	0.0006	0

Table 2 Reference values of standard electrode potential and overpotential

Electrode potential	Value/V
$\varphi^{\Theta}(O_2\|OH^-)$	0.401
$\varphi^{\Theta}(H^+\|H_2)$	0.00
$\varphi^{\Theta}(Pd^{2+}\|Pd)$	0.95
$\varphi^{\Theta}(Pt^{4+}\|Pt)$	1.43
$\varphi^{\Theta}[(RuNO)^{3+}\|Ru)]$	0.46
$\eta(O_2\|Pt)$	0.45
$\eta(H_2\|Ni)$	0.21

activity of electrode reaction substance; η is the overpotential of substance precipitated on electrode; $(a^{\nu})_{\text{reduction station}}$ is the concentration of reduction station; $(a^{\nu})_{\text{oxidation station}}$ is the concentration of oxidation station.

According to Eq. (10), the minimum evolution potential required for each electrode reaction was calculated, and the results are shown in Table 3. The results show that the difference between the maximum evolution potential on the anode and the minimum evolution potential on the cathode is only 1.89 V when the coating rate reaches 1 V/s. In the preparation of the Al_2O_3-Pd and Al_2O_3-Ru composite coatings by CPED, the time difference in the electrode reactions is less than 2 s. Thus, the abovementioned electrode reactions are considered to occur simultaneously and there is no competition relationship between the electrode reactions. Therefore, CPED enables the precious metal to grow throughout the deposition process. Dispersion distribution in the coating can also be achieved.

Fig. 4 illustrates the schematic diagrams of CPED process, and three stages can be divided. The effect of precious metal addition on the deposition process is illustrated by a series of current density-voltage curves of CPED process with the $Al(NO_3)_3 \cdot 9H_2O$ system, as shown in Fig.5.

The first stage is a linear stage, where the current density is increased linearly with the increase in voltage. During CPED process, H_2 is produced at the cathode surface, which promotes the hydrolysis of Al^{3+} and generates a large amount of $Al(OH)_3$. A very small amount of precious metal, such as Pd or Ru, is deposited because of the time constraints of the first stage.

The second stage is the formation of closed gas sheaths, during which the current density decreases and becomes constant. The conductivity of the solution near the cathode surface is almost zero. Thus, the rate of the cathodic reaction becomes very slow.

The third stage is plasma discharge, where the plasma begins to discharge and the current density begins to increase. At this stage, $Al(OH)_3$ is converted into Al_2O_3 by the huge energy of plasma, and the precious metal particles also begin to grow at the cathode to form the composite coating. With the gradual thickening of composite coating, the electrical conductivity is decreased continuously, whereas the critical breakdown field strength of the coating is increased gradually. Meanwhile, the energy density of the arc on the cathode surface gradually decreases, and the current density begins to decrease and finally becomes stable. Eventually, the arcing is

Table 3 Minimum evolution potentials of electrode reactions (V)

Electrode potential	$Al(NO_3)_3$-Pd	$Al(NO_3)_3$-Ru	$Al(NO_3)_3$-Pt
$\varphi(O_2\|OH^-)$	1.53	1.53	1.53
$\varphi(H^+\|H_2)$	−0.36	0.36	0.36
$\varphi(Pd^{2+}\|Pd)$	0.86	-	-
$\varphi[(RuNO)^{3+}\|Ru)]$	-	0.37	-
$\varphi(Pt^{4+}\|Pt)$	-	-	1.38
Negative anode precipitation potential difference	1.89	1.89	1.89

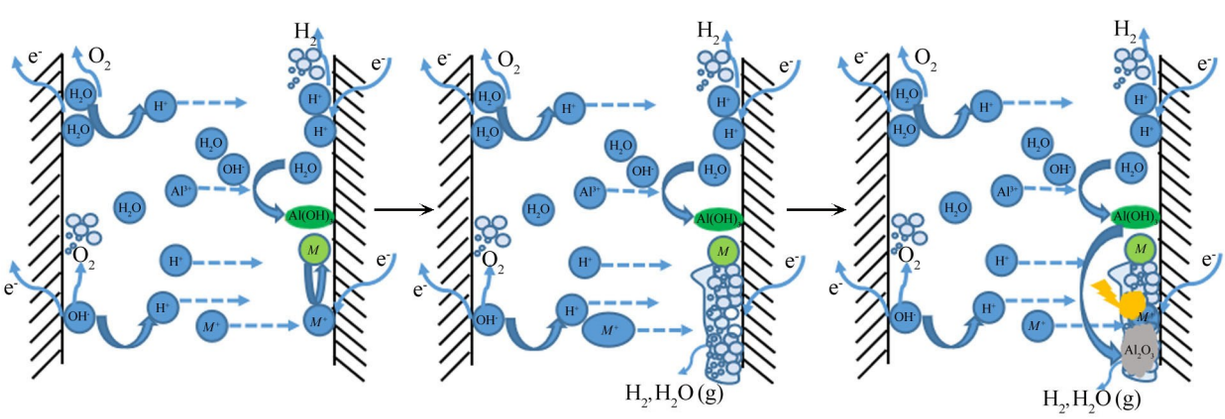

Fig.4 Schematic diagrams of CPED preparation process of Al_2O_3-*M* coatings

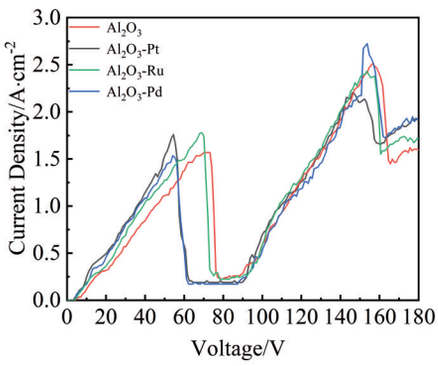

Fig.5 Current density-voltage relationship in CPED process with $Al(NO_3)_3 \cdot 9H_2O$ system with different precious metals

basically stopped, and the composite coating is completely deposited. When the composite coating begins to form on the cathode surface, the dielectric material changes from the original continuous gas sheath to a two-layer structure consisting of a continuous gas sheath and an Al_2O_3-Pd (or Al_2O_3-Ru) composite coating. According to the Maxwell-Wagner model, the electric field strength of the gas sheath (E_{gas}) and the electric field strength of the coating ($E_{coating}$) are not equal to the average electric field strength (E) [16]. The relationships can be expressed as follows:

$$E_{gas} = \frac{\alpha_{coating}(d_{gas} + d_{coating})}{\alpha_{gas} d_{coating} + \alpha_{coating} d_{gas}} E \quad (11)$$

$$E_{coating} = \frac{\alpha_{gas}(d_{gas} + d_{coating})}{\alpha_{gas} d_{coating} + \alpha_{coating} d_{gas}} E \quad (12)$$

where α_{gas} is the electrical conductivity of the gas sheath, $\alpha_{coating}$ is the electrical conductivity of the coating, d_{gas} is the thickness of the gas layer, and $d_{coating}$ is the thickness of the coating layer.

According to Eq. (11 – 12), E_{gas} is greater than $E_{coating}$ because the electrical conductivity of the gas layer is lower than that of the coating layer. In addition, the critical breakdown electric field strength of the gas sheath (approximately 3 MV/m) is much lower than that of the oxide coating (9.9–15.8 MV/m)[16]. Therefore, the gas sheath is broken firstly. When the gas sheath breaks down, the voltage is mainly concentrated on the composite coating, so the electric field strength on the coating increases. In addition, the plasma temperature is as high as 2000 °C or even higher. This high temperature plasma bubble is surrounded by a relatively cold electrolyte (water boiling point), resulting in the rapid plasma cooling. Therefore, the plasma bubble releases a large amount of energy onto the coating surface, resulting in the porous structure of the coatings, as shown in Fig.2.

Under the same electrolyte concentration and voltage, the plasma energy density is basically the same, so the plasma temperature is basically the same. The melting points of Pt, Pd, and Ru are 1768, 1554, and 2250 °C, respectively. Under the plasma, Ru melts less and it is slightly bombarded from the coating, so Ru is more diffusely distributed in the Al_2O_3 coating. Therefore, the critical field strength of the Al_2O_3-Ru composite coating is lower than that of Al_2O_3-Pd composite coating, and its coating porosity is lower. The coating field and plasma energy density reduce when the coatings are prepared at low voltage. More precious metal particles can be deposited in the coating, and the porosity of coatings is larger. However, due to the decrease in plasma energy, the precious metal particles show excessive agglomeration in the coating, as shown in Fig.3a–3c.

2.3 High-temperature cyclic oxidation resistance and thermal effect

Fig. 6 depicts the oxidative kinetics (mass gain) curves and spallation kinetics (spallation mass) curves of different composite coatings. Fig. 6a shows that the mass gain of the sample with Al_2O_3 coating increases rapidly at the beginning of the oxidation period (t<50 h), and the final mass gain is greater than 0.12 mg/cm^2. In contrast, the sample with Al_2O_3-Ru coating exhibits a lower mass gain of approximately 0.08 mg/cm^2. Fig.6b shows that the spallation resistance of the Al_2O_3 coatings is substantially enhanced by the co-deposition of precious metal particles, suggesting that the presence of precious metal particles toughens the Al_2O_3 coatings.

$$K = \frac{m_1 - m_2}{50S} \quad (13)$$

$$G = \frac{m_1 - m_3 - m}{S} \quad (14)$$

where m_1 is the total mass of the sample and the crucible after tests for 100 h; m_2 is the total mass of the sample and the crucible after tests for 50 h; m_3 is the sample mass after tests for 100 h; m is the mass of calcined crucible; S is the area of the sample; K is average oxidation rate; G is average amount of oxide spallation.

According to Eq. (13 – 14), the average oxidation rates of

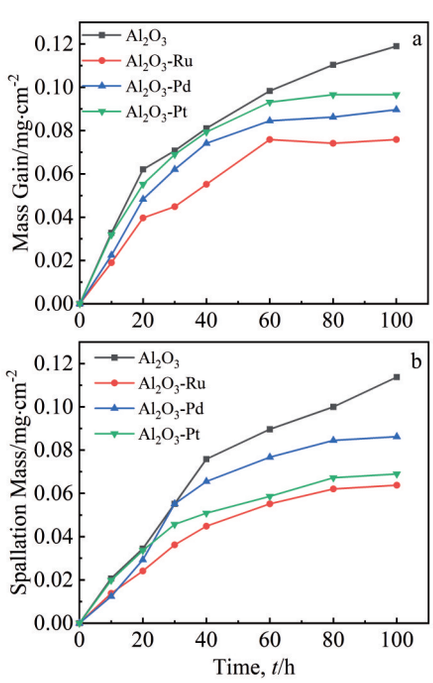

Fig.6 Oxidation kinetics curves (a) and spallation kinetics curves (b) of different Al_2O_3 coatings prepared by CPED at 150 V

different coatings (150 V) are calculated, and the results are shown in Table 4.

It is apparent that the Al_2O_3 coatings containing dispersed precious metal particles have better resistance against the high-temperature oxidation and spallation, compared with Al_2O_3 coating. Comparing the high-temperature oxidation resistance of Al_2O_3-Pt, Al_2O_3-Pd, and Al_2O_3-Ru coatings, the Al_2O_3-Ru composite coating shows optimal properties, and its values of K and G are minimum. Because the Ru particles are more distributed in the Al_2O_3 coating, the porosity of the resultant composite coating is lower. Therefore, its resistance against the high-temperature oxidation is better. Three reasons support the abovementioned results, as follows.

(1) Because precious metal particles have high melting points and thermodynamic stability, they do not react physically or chemically with Al_2O_3 at high temperatures.

(2) There is a blocking effect caused by the composite coating. Ref.[17] reported that the oxygen diffusion along the grain boundary of Al_2O_3 is a control step to determine the oxygen diffusion rate of the coating. The precious metal particles dispersed at the grain boundary have extremely low oxygen diffusion coefficients. Thus, the short-circuit diffusion of oxygen in the external environment at the grain boundary of the Al_2O_3 coating is blocked. Additionally, the grain size of the Al_2O_3 coating decreases after the addition of precious metal particles[18]. Meanwhile, the grain boundary density increases, the diffusion distance of oxygen in the coating becomes longer, and the oxygen diffusion rate decreases accordingly. Therefore, the precious metal-doped oxide ceramic composite coatings show good resistance against high-temperature oxidation.

(3) Precious metal particles provide a toughening effect. The cracking and peeling of the coating at high temperatures are caused by the crack propagation, but precious metal

Table 4 High-temperature oxidation resistance and spallation resistance of different Al_2O_3 coatings prepared by CPED at 150 V

Coating	m_1/g	m_2/g	m_3/g	m/g	K/g·cm^{-2}	G/g·cm^{-2}
Al_2O_3-Pt	7.695 02	7.694 95	4.341 62	3.353 00	0.002 413	0.689 7
Al_2O_3-Ru	8.273 01	8.272 96	4.305 06	3.967 58	0.001 724	0.637 9
Al_2O_3-Pd	8.165 67	8.165 61	4.281 44	3.883 73	0.002 069	0.862 1
Al_2O_3	8.424 10	8.423 95	4.485 50	3.937 84	0.005 172	1.310 3

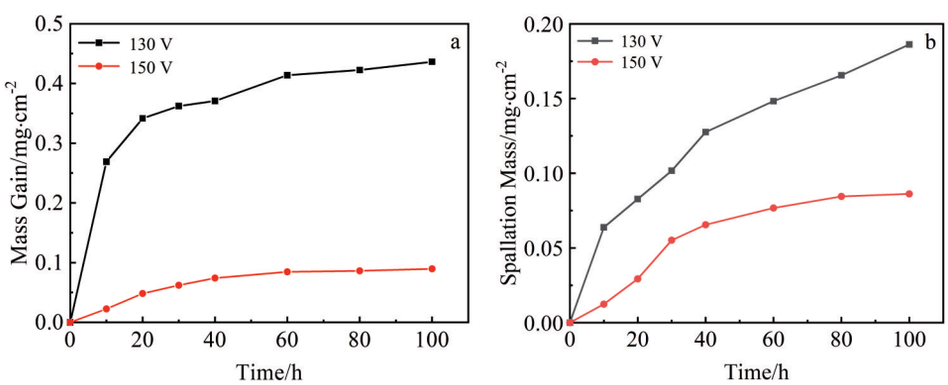

Fig.7 High-temperature oxidation resistance (a) and spallation resistance (b) of Al_2O_3-Pd coatings prepared at different voltages after cyclic oxidation test at 1273 K for 100 h

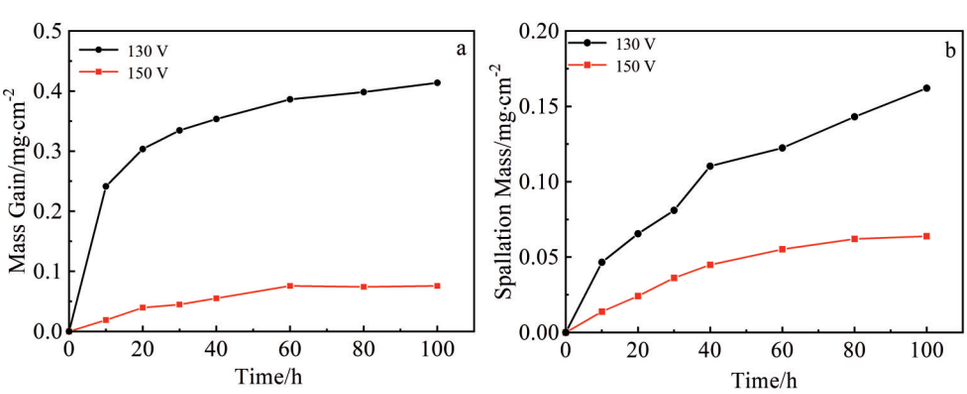

Fig.8 High-temperature oxidation resistance (a) and spallation resistance (b) of Al_2O_3-Ru coatings prepared at different voltages after cyclic oxidation test at 1273 K for 100 h

particles can absorb the energy of crack propagation by plastic deformation, preventing the crack expansion and achieving the toughening effect by sealing cracks and reducing defects in the coating[19]. These results jointly improve the high-temperature peeling resistance of the composite coating.

Fig. 7 and Fig. 8 show the high-temperature oxidation resistance of the composite coatings prepared at different voltages. The performance of the coatings prepared at 130 V is inferior. On the one hand, the low voltage is not conducive to the dispersing of precious metal particles. The inferior adhesion of the coating reduces the oxidation resistance of the composite coating. On the other hand, because the precious metal particles agglomerate, the oxygen transmission channels may be formed to reduce the oxidation resistance of the coatings.

3 Conclusions

1) The high-temperature oxidation resistance and spallation resistance of the Al_2O_3-Pt, Al_2O_3-Pd, and Al_2O_3-Ru composite coatings are improved by the dispersion distribution of precious metals.

2) The Al_2O_3-Ru composite coating shows optimal performance with the minimum average oxidation rate and the minimum average amount of oxide spallation.

References

1 Ogita Y I, Ohsone S, Kudoh T *et al*. *Thin Solid Films*[J], 2008, 516(5): 836

2 Wang J, Binner J, Pang Y *et al*. *Thin Solid Films*[J], 2008, 516(18): 5996

3 Musil J, Blažek J, Zeman P *et al*. *Applied Surface Science*[J], 2010, 257(3): 1058

4 Wei X L, Xia Y, Liu X M *et al*. *Electrochimica Acta*[J], 2014, 136: 250

5 Gupta P, Tenhundfeld G, Daigle E O *et al*. *Surface & Coatings Technology*[J], 2007, 201(21): 8746

6 Yerokhin A L, Nie X, Leyland A *et al*. *Surface & Coatings Technology*[J], 1999, 122(2–3): 73

7 Yang X, Ding X F, Hao G J *et al*. *Plasma Chemistry & Plasma Processing*[J], 2016, 37: 177

8 Liu C X, Zhang J, Zhang S G *et al*. *Surface & Coatings Technology*[J], 2017, 325: 708

9 Yerokhin A, Pilkington A, Matthews A. *Journal of Materials Processing Technology*[J], 2010, 210(1): 54

10 Liu C X, Zhao Q, Wang L X *et al. RSC Advances*[J], 2017, 7(63): 39824

11 Zhou S, He Y D, Wang D R *et al*. *Transactions of Materials & Heat Treatment*[J], 2013, 34(12): 171

12 Wang Y, Jiang Z, Liu X *et al*. *Applied Surface Science*[J], 2009, 255(21): 8836

13 Bahadori E, Javadpour S, Shariat M H *et al*. *Surface & Coatings Technology*[J], 2013, 228(9): S611

14 Zhang Y P, Meng Y, Shen Y H *et al*. *Applied Surface Science*[J], 2017, 419(15): 357

15 Wang P, He Y D, Zhang J. *Materials Chemistry & Physics*[J], 2016, 184: 1

16 Liu C X, Zhang J, He Y D *et al*. *Materials Research Express*[J], 2017, 4(3): 036306

17 Wang P, He Y D, Deng S J *et al*. *International Journal of Minerals, Metallurgy and Materials*[J], 2016, 23(1): 92

18 Deng S J, Wang P, He Y D *et al*. *International Journal of Minerals, Metallurgy and Materials*[J], 2016, 23(6): 704

19 Bunget I, Popescu M. *Physics of Solid Dielectrics*[M]. Amsterdam: Elsevier, 1984

阴极等离子电解沉积制备 Al_2O_3-Ru 复合涂层的机理与性能

薛建超[1,2]，贾　波[2]，王亚菲[2]，冯　庆[2]，柴作强[2]，郝小军[2]，薛娟琴[1]

(1. 西安建筑科技大学 冶金工程学院，陕西 西安 710055)

(2. 西安泰金新能科技股份有限公司，陕西 西安 710016)

摘　要：采用阴极等离子体电沉积法制备了不同贵金属掺杂氧化铝涂层。结果表明，贵金属掺杂氧化铝制备的涂层孔隙率降低（特别是Al_2O_3-Ru），涂层的耐高温循环氧化性能和抗剥落性能均有所提升。Al_2O_3-Ru复合涂层的效果更好，平均氧化速率值K和平均氧化物碎裂量G最小。同时，利用能斯特方程解释了贵金属和氧化铝同时沉积的原因，对沉积的整个过程和机理进行了分析和探讨。

关键词：阴极等离子电解沉积；贵金属；孔隙率；耐高温循环氧化；抗剥落性能

作者简介：薛建超，男，1994年生，博士，西安建筑科技大学冶金工程学院，陕西 西安 710055，电话：029-86968453，E-mail：jianchao_xue@163.com